International Journal of Polymer Analysis and Characterization

ISSN: 1023-666X (Print) 1563-5341 (Online) Journal homepage: http://www.tandfonline.com/loi/gpac20

Morphology, interfacial interaction, and thermal degradation of polycarbonate/MCM-41 (nano)composites

M. A. Sibeko, A. S. Luyt, M. L. Saladino & E. Caponetti

To cite this article: M. A. Sibeko, A. S. Luyt, M. L. Saladino & E. Caponetti (2017): Morphology, interfacial interaction, and thermal degradation of polycarbonate/MCM-41 (nano)composites, International Journal of Polymer Analysis and Characterization, DOI: 10.1080/1023666X.2017.1313808

To link to this article: http://dx.doi.org/10.1080/1023666X.2017.1313808

Accepted author version posted online: 10 Apr 2017.
Published online: 10 Apr 2017.

INTERNATIONAL JOURNAL OF POLYMER ANALYSIS AND CHARACTERIZATION
https://doi.org/10.1080/1023666X.2017.1313808

Morphology, interfacial interaction, and thermal degradation of polycarbonate/MCM-41 (nano)composites

M. A. Sibeko[a], A. S. Luyt[b], M. L. Saladino[c,d], and E. Caponetti[c,d]

[a]Department of Chemistry, University of the Free State (Qwaqwa Campus), Phuthaditjhaba, South Africa; [b]Center for Advanced Materials, Qatar University, Doha, Qatar; [c]Department of Biological, Chemical and Pharmaceutical Science and Technology - STEBICEF and INSTM UdR - Palermo, University of Palermo, Italy; [d]Center of Large Equipment - ATeN Center, University of Palermo, Palermo, Italy

ABSTRACT

This article reports on the morphology, interfacial interaction, thermal stability, and thermal degradation kinetics of polycarbonate (PC)/mesoporous silica (MCM-41) composites with various MCM-41 contents, prepared by melt compounding. The composites with low filler loadings (<0.3 wt%) maintained their transparency because of the well dispersed MCM-41 particles, but at higher filler loadings the composites lost their transparency due to the presence of agglomerates. The presence of agglomerates decreased the thermal stability of PC due to the reduced effectiveness of the particles to immobilize the polymer chains, free radicals, and volatile degradation products.

ARTICLE HISTORY
Submitted 6 March 2017
Accepted 29 March 2017

KEYWORDS
Mesoporous silica; nanocomposites; polycarbonate; structure–property relationship; thermal degradation

Introduction

Over the past decades, optically transparent polymers attracted considerable attention in numerous applications including protective face shields, eyewear, and electronic display screens. In other sectors, such as construction materials or fire safety equipment, both good transparency and fire resistance properties are needed.[1–3] Polycarbonate (PC) is a well-known engineering thermoplastic with a high molecular weight and impact strength. It combines toughness, heat resistance, flame resistance, and dimensional stability. However, because of its high melt viscosity and poor resistance to abrasion and chemicals, it is not suitable for certain applications, so its properties can be improved by blending it with other polymers or by adding nanoparticles. The introduction of nanoparticles had been widely investigated and reported to be the most efficient method to improve the properties of PC.[1,4–7] Various fillers, which included graphite,[8] metal oxide nanoparticles,[9–11] carbon black,[12] nanoclays,[13] and carbon nanotubes,[14] were investigated as possible PC reinforcement.

Recently, researchers started to use mesoporous silica (MCM-41) particles as additives into polymers, due to the possibility of improving the electrical conductivity, as well as the mechanical and thermal properties, of the polymers. MCM-41 particles were discovered about 20 years ago and investigated for their properties such as nanometric pore size, large surface area, and pore volume, which made them to be suitable to be used as catalyst and adsorbent materials. The most investigated is MCM-41, which is normally prepared by a sol–gel method in the presence of a surfactant or template. After the formation of the MCM-41 particles, the template is removed to obtain the porous structure.[15–17]

Mesoporous silica had been used as additive for various polymers that include poly(ethylene terephthalate) (PET),[18] polyethylene,[19] polystyrene,[20] polypropylene,[21] natural rubber,[22] poly

CONTACT A. S. Luyt aluyt@qu.edu.qa Center for Advanced Materials, Qatar University, P.O. Box 2713, Doha, Qatar.
Color versions of one or more of the figures in this article can be found online at www.tandfonline.com/gpac.

(methyl methacrylate) (PMMA),[23] and polyurethane.[24] In general, the addition of MCM-41 increased the thermal stability of a number of these polymers, and this was generally attributed to the good thermal stability of the MCM-41 nanoparticles, and to the interaction between the polymer chains and the internal surfaces of the pores in MCM-41. Composites prepared with MCM-41 (with template) showed better thermal stability than the MCM-41 (without template) composites, because the polymer and the template mixture enhanced the interaction through entanglement and inter-diffusion, thus forming a network which enhanced the thermal stability.[25]

Some researchers explained the improved thermal stability to the insertion of the polymeric chains inside the mesopores or to the fact that the porous structure trapped the volatile degradation products or acted as scavenger of radical species during the degradation process.[26,27] It was also stated that a mobility decrease of the polymer chains, trapped in the pores, increased the storage modulus.[10,20,22,28] Contradictory results were reported, where the addition of nanoparticles in PC showed increases,[5,6,13] decreases,[29–31] or no significant effects[32] on the thermal stability of PC. Maiti et al.[6] related an increase in the thermal stability of PC with the addition of multiwalled carbon nanotubes (MWCNTs) to the restriction of the mobility of the polymer chains near the nanofiller surface. During combustion the MWCNTs also acted as inflammable anisotropic nanoparticles, forming a jammed network of char layers that retarded the transport of the decomposition products. Vani et al.[5] related the increase in thermal stability to the confinement of PC chains in the clay galleries that delayed the diffusion of volatile products and the degradation process. A decrease in the thermal stability with the addition of TiO_2, ZrO_2, and ZnO was related to a catalytic effect of the nanoparticles, the state of nanoparticles dispersion in the polymer matrix, and the preparation conditions. Several groups investigated the dynamic mechanical properties of PC composites.[2,5,11,13] An increase in storage and loss modulus was attributed to the reinforcing effect of the nanofillers as a result of their high aspect ratios, or the formation of crystalline domains around the nanoparticles that effectively improved the interaction between the particles and the PC chains.

As mentioned above, a number of papers reported different and sometimes contradictory results concerning the effect of nanoparticles on the thermal stability of PC. To get a better understanding of the degradation process and the effect of the MCM-41 loading on the thermal stability of PC, this paper reports on the effect of MCM-41 on the morphology, interfacial interaction, thermal stability, and thermal degradation kinetics of PC. Thermogravimetric analyses (TGA) were performed to investigate the degradation kinetics, whereas transmission electron microscopy (TEM) and small-angle X-ray scattering (SAXS) techniques were applied to correlate the changes in the properties with the morphology and structure of the composites. ^{13}C cross-polarization magic-angle spinning NMR (^{13}C (^{1}H) CP-MAS NMR) measurements were used to establish any chemical or physical interaction between the PC and MCM-41.

Materials and methods

Materials

Commercial grade bisphenol-A polycarbonate (Makrolon® 2407), with a melt flow rate of 20 g/10 min at 300°C/1.2 kg, and $M_w = 57\ 404\ g\ mol^{-1}$, was obtained in pellet form from Bayer Material Science, Germany. MCM-41, with a surface area of ~1,000 $m^2\ g^{-1}$, pore sizes ranging between 2.1 to 2.7 nm, and a pore volume of 0.98 $cm^3\ g^{-1}$, was supplied by Sigma-Aldrich and used as received.

Preparation of the PC/MCM-41 composites

Polycarbonate pellets and MCM-41 powder were dried in an oven at 80°C for 12 h before preparation. The composites were prepared in the same way as our previously reported PMMA/MCM-41 composites.[28] All the composites were prepared using a Brabender Plastograph 50 ml melt-mixer at 200°C and 50 rpm for 10 min. For the preparation of the composites, PC was first melted for

2 min at 200°C, and different contents (0.1, 0.3, 0.5, 1, 2, and 5 wt%) of the MCM-41 were added into the molten polymer and mixed for a further 8 min. The samples were then melt pressed into 3 mm thick sheets at 200°C for 5 min at 50 bar. Pure PC as the control sample, was treated similarly.

Sample analysis

Transmission electron microscopy micrographs were acquired using a JEM-2100 (JEOL, Japan) electron microscope operating at 200 kV accelerating voltage. For the observation of the composites, 100 nm thick slices were prepared by using a Leica EM UC6 ultra-microtome, and were put onto a 3 mm Cu grid "lacey carbon" for analysis.

Small angle X-ray scattering measurements were performed using a Bruker AXS Nanostar-U instrument, with a Cu rotating anode working at 40 kV and 18 mA. The X-ray beam was monochromatized at a wavelength $\lambda = 1.54056$ Å (Cu Kα) using a couple of Göbel mirrors, and was collimated using a series of three pinholes with diameters of 500, 150, and 500 µm. Samples were directly mounted on the sample stage to avoid additional scattering of the holder. Data were collected at room temperature for 5,000 s by using a two-dimensional multiwire proportional counter detector placed at 24 cm from the sample, allowing the collection of data in the Q scattering vector ($Q = 4\pi \sin \theta/\lambda$) range of 0.02–0.78 $Å^{-1}$.

The ^{13}C (^{1}H) CP-MAS NMR spectra were obtained at room temperature using a Bruker Avance II 400 MHz (9.4 T) spectrometer operating at 100.63 MHz for the ^{13}C nucleus with a MAS rate of 10 kHz, 400 scans, a contact time of 1.5 µs, and a repetition delay of 2 s. The optimization of the Hartmann–Hahn condition was obtained using an adamantane sample. Each sample was placed in a 4 mm zirconia rotor with KEL-F caps using silica as filler to avoid inhomogeneities inside the rotor. The proton spin–lattice relaxation time in the rotating frame $T_{1\rho}(H)$ was indirectly determined, with the variable spin lock (VSL) pulse sequence, by the carbon nucleus observation using a 90°-τ-spin-lock pulse sequence prior to cross-polarization with a delay time τ ranging from 0.01 to 3 s. The ^{13}C spin–lattice relaxation time in the rotating frame $T_{1\rho}(C)$ was determined, with the VSL pulse sequence, applying the spin-lock pulse after the cross-polarization on the carbon channel. The data acquisition was performed by ^{1}H decoupling with a spin lock pulse length, τ, ranging from 0.4 to 30 ms and a contact time of 1.5 ms.

A PerkinElmer STA6000 TGA was used to analyze the thermal degradation behavior of the samples. The analyses were done from 30 to 700°C at a heating rate of 10°C min^{-1} under nitrogen flow (20 ml min^{-1}). The sample masses ranged between 20 and 25 mg. The samples for thermal degradation kinetics were run at 3, 5, 7, and 9°C min^{-1} heating rates under nitrogen flow (20 ml min^{-1}), and the TGA's integrated kinetics software [based on the Flynn–Ozawa–Wall method (Equation 1)] was used to calculate the activation energies:

$$\ln \beta = c - 1.052\left(\frac{E_a}{RT}\right) \tag{1}$$

where β is the heating rate in K min^{-1}, c is a constant, E_a is the activation energy in kJ mol^{-1}, R is the universal gas constant, and T is the temperature in K. The plot of ln β versus $1/T$, obtained from the TGA curves recorded at several heating rates, should be a straight line. The activation energy was evaluated from its slope.

Results and discussion

Morphology and structure of the composites

Transmission electron microscopy micrographs were acquired to investigate the filler dispersion in the polymer. The MCM-41 powder presented well-ordered channels with a hexagonal symmetry typical of the mesoporous structure.[28] The TEM micrographs of the PC/MCM-41 composites loaded

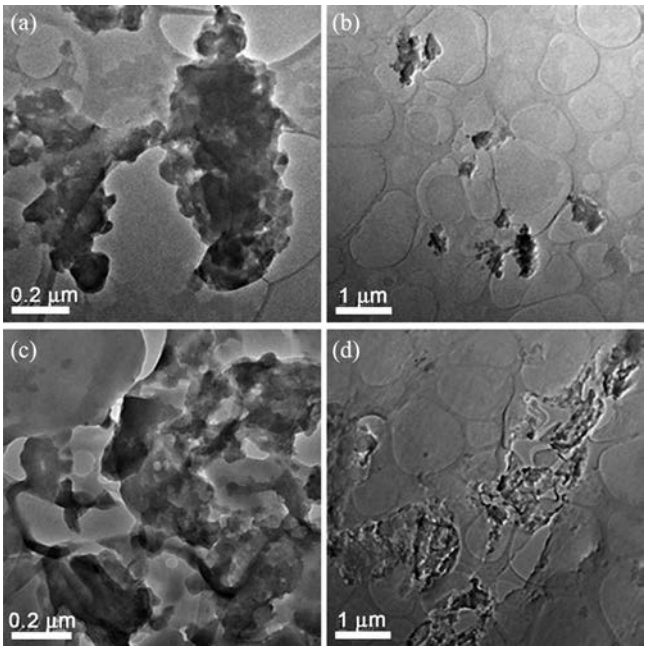

Figure 1. TEM micrographs of the PC/MCM-41 composites with 0.5 wt% (a,b) and 5 wt% (c,d) loading at different magnifications.

with 0.5 and 5 wt% MCM-41 are shown in Figure 1. Figure 1a shows an agglomerated MCM-41 particle in the polymer, and these agglomerates are well dispersed in the polymer matrix (Figure 1b). Figure 1c and d show poorly dispersed and highly agglomerated MCM-41 particles, and this caused the decrease in transparency of the composites at higher MCM-41 content, as observed in Figure 2.

The SAXS patterns of the investigated samples, after background and thickness corrections, are shown as a function of the scattering vector Q in Figure 3. The SAXS pattern of MCM-41 was reported in our previous paper,[28] and it showed an intense (100) peak at 0.15 $Å^{-1}$ and two low-intensity reflections ((110) at 0.26 $Å^{-1}$ and (200) at 0.32 $Å^{-1}$) that are characteristic of hexagonal structures. The SAXS measurements, performed on different portions of the samples, gave the same results, which confirmed the homogeneity of the samples.

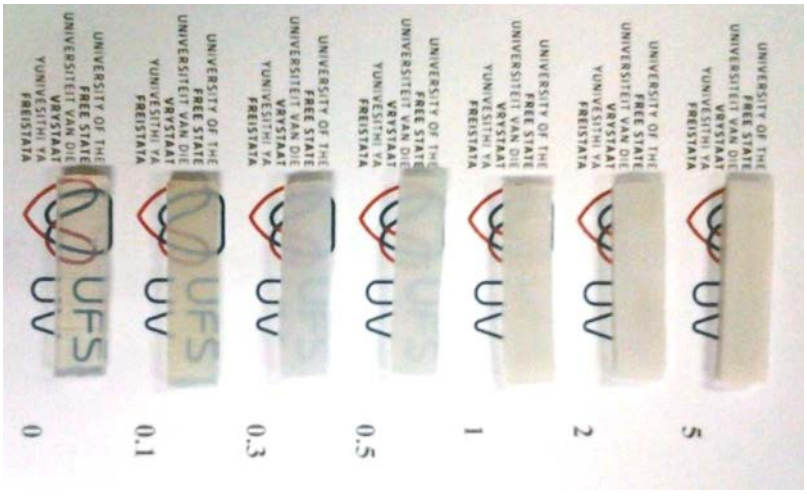

Figure 2. Samples of PC/MCM-41 composites containing different amounts of MCM-41 showing the decrease in transparence with increasing MCM-41 content.

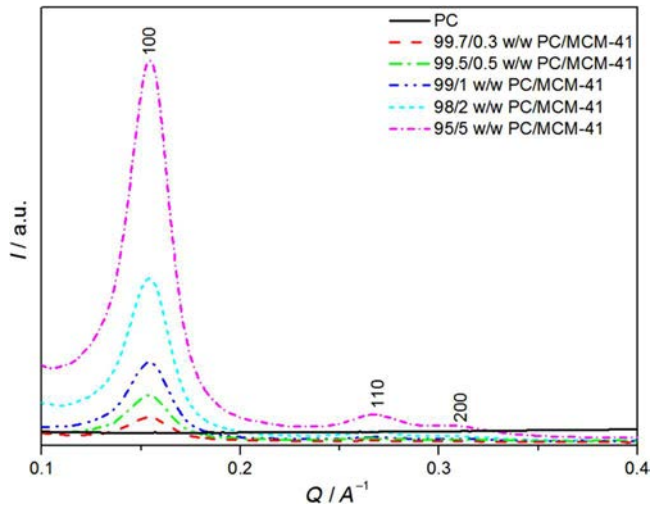

Figure 3. SAXS intensities versus scattering vector Q of MCM-41 and the PC/MCM-41 composites.

The SAXS pattern of the pure PC does not show any peak in the investigated scattering intensity $I(Q)$ range, because it is an amorphous polymer, whereas the PC/MCM-41 composites show the three characteristic peaks of MCM-41, indicating that the MCM-41 maintained its hexagonal lattice symmetry after composite formation. d_{100} and a_0 for MCM-41 had been calculated as 4.1 and 4.8 nm, respectively.[28] No shift in the (100) peak was observed after composite formation, indicating that the pore size of the mesoporous materials did not vary. There is a possibility that the polymer chains (or parts of it) may penetrate the pores of the MCM-41 during the preparation process of the polymer/mesoporous filler composites.[33,34] To check whether this is probable for our system, we calculated the radius of gyration for the PC we used, and based on the value we obtained and on work done by the group of Müller et al.[35–37] where it was shown that the radius of gyration must be significantly smaller than the a_0 value of nanoporous fillers for the polymer chains to be able to penetrate the pores, we disregarded this as a possible mechanism for the immobilization of the PC chains in the PC/MCM-41 composites.

Interactions between PC chains and the MCM-41 filler

The peaks in the ^{13}C (^{1}H) CP MAS NMR spectra of PC and the PC/MCM-41 composites loaded with 0.5 and 5 wt% MCM-41 in Figure 4 are numbered to show the assignment of the ^{13}C chemical shifts of the polymer. All the spectra show five resonances, peak 1 at 149 ppm is related to the quaternary carbons of the aromatic rings and to the carbonyl carbon, peak 2 at 127 ppm to the aromatic carbon meta to the oxygen, peak 3 at 120 ppm to the aromatic carbon ortho to the oxygen, peak 4 at 42 ppm to the quaternary carbon bonded to the methyl groups, and peak 5 at 31 ppm to the methyl carbons.

The presence of MCM-41 did not induce any modification in the chemical shift and signal shape, indicating that no new chemical bond was formed during composite preparation. To investigate the physical interaction between the two components in the composite and to detect dynamic changes in the polymer induced by the MCM-41, the proton and carbon spin lattice relaxation times in the rotating frame, $T_{1\rho}(H)$ and $T_{1\rho}(C)$, were determined. These values are reported in Table 1. The presence of MCM-41 at 0.5 and 5 wt% loading did not significantly affect the $T_{1\rho}(H)$ values, but the relaxation time for the carbonyl carbon peak (peak 1) increased at 5 wt% MCM-41 loading. This is the evidence that the interaction between the MCM-41 and the polymer matrix was principally localized in this nuclear environment. However, the $T_{1\rho}(C)$ values were affected by the presence of MCM-41. The carbon 1 value for PC decreased after the addition of 0.5 wt% MCM-41, but at the higher filler loading it increased, not

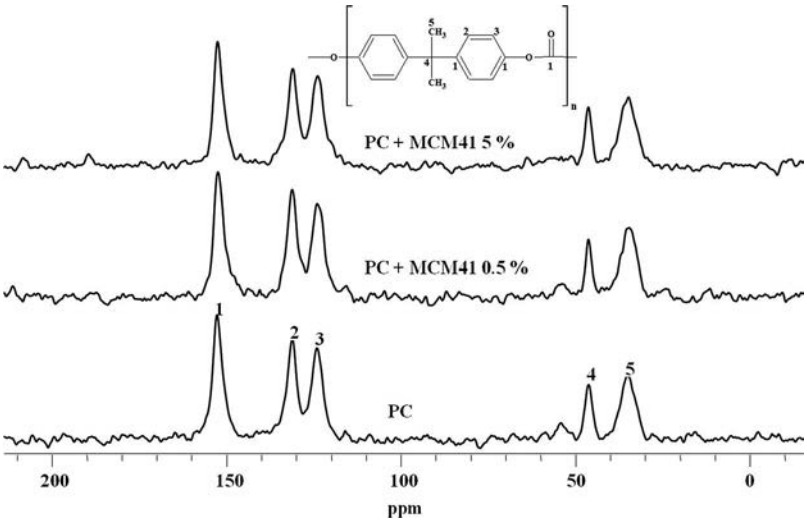

Figure 4. ^{13}C (^{1}H) CP-MAS NMR spectra of PC and of the PC/MCM-41 composites.

Table 1. Relaxation time values for all the peaks in the ^{13}C spectra of PC and the PC/MCM-41 composites loaded with 0.5 and 5 wt% of MCM-41.

		$T_{1\rho}H$ (ms)			$T_{1\rho}C$ (ms)		
Carbon	ppm	0 wt%	0.5 wt%	5 wt%	0 wt%	0.5 wt%	5 wt%
1	149	4.9 ± 0.2	4.9 ± 0.2	6.0 ± 0.2	95.3 ± 0.3	38.8 ± 0.4	102.9 ± 0.2
2	127.5	4.9 ± 0.2	5.2 ± 0.2	5.4 ± 0.3	10.9 ± 0.2	11.1 ± 0.2	10.6 ± 0.2
3	120	4.4 ± 0.2	5.6 ± 0.2	4.4 ± 0.2	11.2 ± 0.2	10.9 ± 0.2	29.1 ± 0.2
4	42	3.9 ± 0.2	4.2 ± 0.2	4.5 ± 0.3	28.4 ± 0.3	31.6 ± 0.2	55.6 ± 0.2
5	31	6.6 ± 0.3	4.9 ± 0.2	5.9 ± 0.2	30.5 ± 0.2	23.2 ± 0.2	20.5 ± 0.2

only for carbon 1 but also for carbons 3 and 4. These increases can be attributed to a restriction in the mobility of the polymer chains. The carbonyl carbon is particularly hindered because of a specific interaction which is probably hydrogen bonding with the Si–OH groups on MCM-41.[38,39]

Thermal degradation

The addition of MCM-41 up to 1 wt% increased the thermal stability of PC (Figure 5, Table 2). The pores would trap the volatile degradation products and delay their diffusion out of the polymer, so that they were only released at higher temperatures. Mingtao et al.[25] also observed an increase in the thermal stability of PET in the presence of mesoporous molecular sieves. They related the increase to the presence of polymer chains in the mesoporous channels, making them more stable due to the protection of the inorganic pore-wall. In our case the polymer and free radical chains were more probably immobilized through their hydrogen-bonding interaction with the small and well dispersed filler particles, which would delay the propagation of the degradation reaction. The sample with 5 wt% MCM-41, however, shows a decrease in mass loss temperature to a value approximately the same as that of pure PC. This can be attributed to the agglomerates observed in the TEM micrographs, which reduced the effectiveness of the filler particles to immobilize the polymer and free radical chains, and the volatile degradation products. Motaung et al.[32] studied the same system, but used nonporous silica particles at 1, 2, and 5 wt% loadings. They observed an insignificant increase in thermal stability with the addition of 1 and 2 wt% silica, while a decrease in the thermal stability was observed for the sample containing 5 wt% silica. The thermal stability of the composites at 5 wt% silica was lower than that of the pure polymer, and they attributed the decrease to the catalytic effect of the silica particles. Carrion et al.[31] observed lower decomposition temperatures

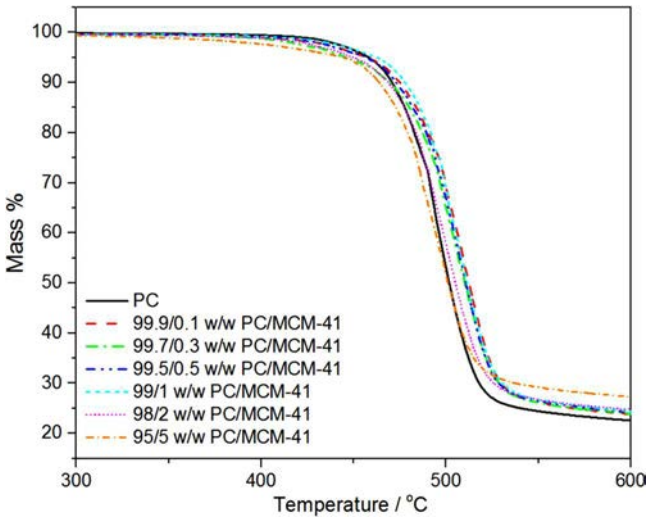

Figure 5. TGA curves of PC and the PC/MCM-41 composites.

Table 2. TGA results for PC and the PC/MCM-41 composites.

Sample	T_{30}/°C	T_{max}/°C	% Residue
PC	491.6	496.3	22.2
99.9/0.1 w/w PC/MCM-41	499.2	510.2	23.8
99.7/0.3 w/w PC/MCM-41	496.7	508.4	23.8
99.5/0.5 w/w PC/MCM-41	497.7	509.4	24.2
99/1 w/w PC/MCM-41	500.3	508.1	24.5
98/2 w/w PC/MCM-41	491.9	502.6	24.9
95/5 w/w PC/MCM-41	487.4	497.6	27.3

for PC heated in the presence of ZnO nanoparticles at 0.1, 0.5, 1, and 5 wt% loading, which they attributed to the presence of large aggregated nanoparticles.

To get a better understanding of the degradation process and the effect of the MCM-41 loading on the thermal stability of PC, the minimum amount of energy that is required to initiate and propagate

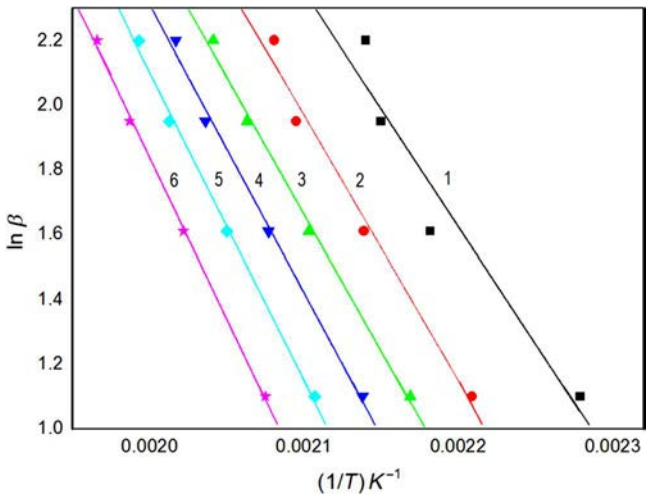

Figure 6. Ozawa–Flynn–Wall plots derived from the PC mass loss curves for the following degrees of conversion: (1) $\alpha = 0.1$; (2) $\alpha = 0.2$; (3) $\alpha = 0.3$; (4) $\alpha = 0.4$; (5) $\alpha = 0.5$; (6) $\alpha = 0.6$.

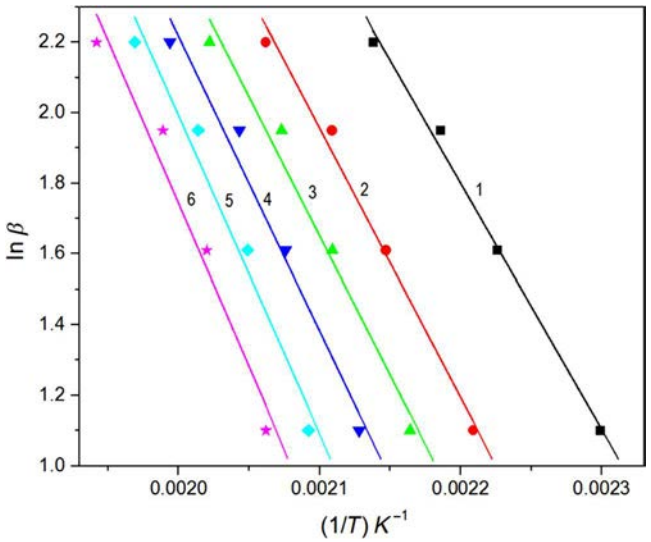

Figure 7. Ozawa–Flynn–Wall plots derived from the 99.5/0.5 w/w PC/MCM-41 mass loss curves for the following degrees of conversion: (1) $\alpha = 0.1$; (2) $\alpha = 0.2$; (3) $\alpha = 0.3$; (4) $\alpha = 0.4$; (5) $\alpha = 0.5$; (6) $\alpha = 0.6$.

the degradation process was determined. The activation energy (E_a) for mass loss was determined from the slope of the isoconversional plots of ln β versus $1/T$ (Figures 6–8) taken from TGA curves obtained at heating rates of 3, 5, 7, and 9°C min^{-1}. The relationship between the activation energy and the extent of mass loss is shown in Figure 9. The activation energy of mass loss for PC and the PC/MCM-41 composites increased with an increase in the extent of mass loss, which means that the degradation process involved multiple steps.[40]

The activation energies of the sample containing 0.5 wt% MCM-41 were higher than that of pure PC, which can be attributed to more energy required for mass loss to occur. As already discussed, this may result from an increase in thermal stability through the immobilization of the polymer and free radical chains by the MCM-41 particles, or through a delay in the diffusion of the volatile degradation products out of the molten sample. However, the sample containing 5 wt% MCM-41 shows lower

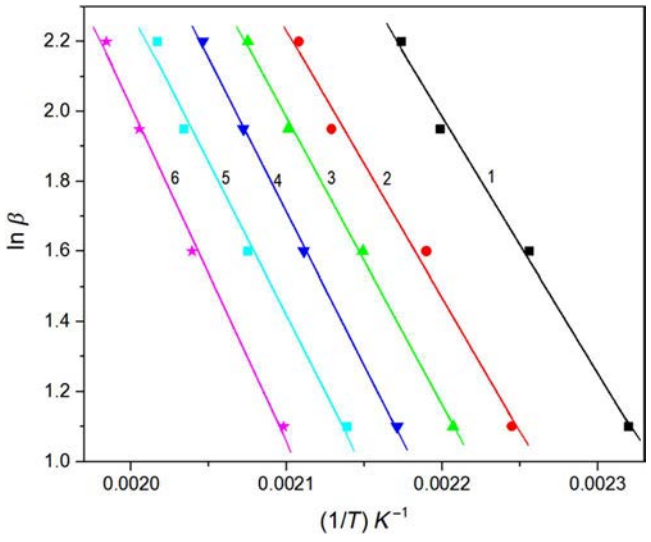

Figure 8. Ozawa–Flynn–Wall plots derived from the 95/5 w/w PC/MCM-41 mass loss curves for the following degrees of conversion: (1) $\alpha = 0.1$; (2) $\alpha = 0.2$; (3) $\alpha = 0.3$; (4) $\alpha = 0.4$; (5) $\alpha = 0.5$; (6) $\alpha = 0.6$.

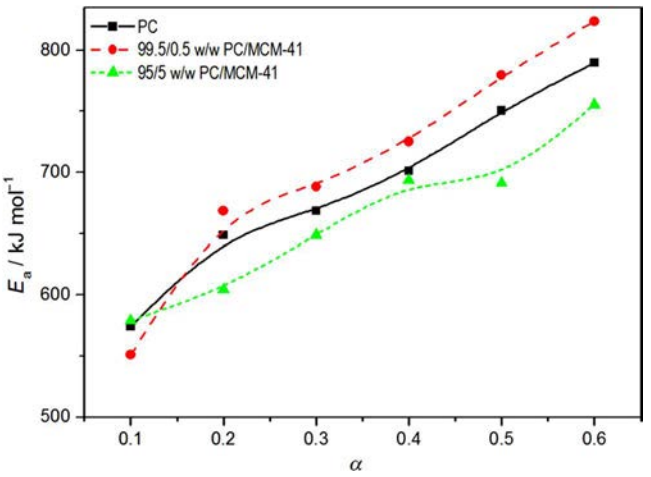

Figure 9. Activation energy versus extent of mass loss for PC and the PC/MCM-41 composites with 0.5 and 5 wt% MCM-41.

activation energy values than pure PC. This could have been the result of (1) a catalytic effect of the larger MCM-41 agglomerates on the PC degradation and/or (2) the creation of more free volume for the diffusion of volatile degradation products out of the sample. Araujo et al.[18] and Motaung et al.[32] attributed similar observations to a catalytic effect of the filler on polymer degradation. MCM-41 can be used as a catalyst because of its large surface areas, ordered pore structures and readily controlled pore diameters.[41] A study of the catalytic effect of the MCM-41 on the thermal degradation kinetics of PET, where 25% (w/w) of MCM-41 was added into the polymer, showed a decrease in the activation energy of degradation of PET, which was related to the catalytic effect of the MCM-41. From our results it seems as if the MCM-41 agglomerates were more effective as degradation catalyst.

Conclusion

The purpose of this work was to investigate the influence of MCM-41 in the range of 0.1–5 wt% on the morphology and thermal degradation behavior of PC. The addition of MCM-41 up to 1 wt% increased the thermal stability of PC, which was probably due to a delayed mass loss because of the trapping of the volatile degradation products in the pores of MCM-41. However, the thermal stability decreased at 5 wt% MCM-41 loading due to the presence of agglomerates, which reduced the effectiveness of the agglomerated filler particles to immobilize the free radical chains and volatile degradation products. There is also the possibility of MCM-41 acting as a catalyst, thus initiating the degradation process of PC.

Funding

The authors acknowledge the University of Palermo for supporting this research through the CORI2013 (Bando per la concessione di contributi per l'avvio e lo sviluppo di collaborazioni dell'Ateneo 2013-Azione D—prot. 32827 del 2/5/2013). SAXS, NMR, and TEM experimental data were provided by Centro Grandi Apparecchiature, Università di Palermo funded by P.O.R. Sicilia 2000–2006, Misura 3.15 Azione C Quota Regionale. The National Research Foundation in South Africa funded the bursary of the student who worked on this project.

References

[1] Vahabi, H., O. Eterradossi, L. Ferry, C. Longuet, R. Sonnier, and J. M. Lopez-Cuesta. 2013. Polycarbonate nanocomposites with improved fire behavior, physical and psychophysical transparency. *Eur. Polym. J.* 49:319–327.

[2] Feng, J., J. Hao, J. Du, and R. Yang. 2012. Effect of organoclay on the flammability, thermal and mechanical properties of polycarbonate nanocomposites filled with a phosphate and organoclays. *Polym. Degrad. Stabil.* 97:108–117.
[3] Wang, Y., B. Wang, Y. Zhao, C. Liu, and J. Chen. 2014. Thermal degradation mechanism and kinetics of polycarbonate/silica nanocomposites. *Polym. Degrad. Stabil.* 107:129–138.
[4] Nevalainen, K., J. Vuorinen, V. Villaman, R. Suihkonen, P. Jarvela, J. Sundelin, and T. Lepisto. 2009. Characterization of twin-screw-extruder-compounded polycarbonate nanoclay composites. *Polym. Eng. Sci.* 49:631–640.
[5] Vani, J., S. S. Mohanty, M. R. Parvaiz, and S. K. Nayak. 2011. Influence of nanoclays and nano-TiO_2 on the mechanical and thermal properties of polycarbonate nanocomposites. *Macromol. Res.* 19:563–572.
[6] Maiti, S., N. K. Shrivastava, S. Suin, and B. B. Khatua. 2013. A strategy for achieving low percolation and high electrical conductivity in melt-blended polycarbonate (PC)/multiwalled carbon nanotubes (MWCNT) nanocomposites: Electrical and thermo-mechanical properties. *eXPRESS Polym. Lett.* 7:505–518.
[7] Asyadi, F., M. Jawaid, A. Hassan, and M. U. Wahit. 2013. Mechanical properties of mica-filled polycarbonate/poly (acrylonitrile-butadiene-styrene) composites. *Polym. Plast. Technol. Eng.* 52:727–736.
[8] Zhang, F., Q. Li, Y. Liu, S. Zhang, C. Wu, and W. Guo. 2016. Improved thermal conductivity of polycarbonate composites filled with hybrid exfoliated graphite/multi-walled carbon nanotube fillers. *J. Therm. Anal. Calorim.* 123:431–437.
[9] Rathore, B. S., M. S. Gaur, and K. S. Singh. 2012. Investigation of optical and thermally stimulated properties of SiO_2 nanoparticles-filled polycarbonate. *J. Appl. Polym. Sci.* 126:960–968.
[10] Rouabah, F., M. Fois, L. Ibos, A. Boudenne, and D. Dadache. 2007. Mechanical and thermal properties of polycarbonate. II. Influence of titanium dioxide content and quenching on pigmented polycarbonate. *J. Appl. Polym. Sci.* 106:2710–2717.
[11] Motaung, T. E., M. L. Saladino, A. S. Luyt, and D. C. Martino. 2013. Influence of the modification, induced by zirconia nanoparticles, on the structure and properties of polycarbonate. *Eur. Polym. J.* 49:2022–2030.
[12] Pötschke, P., M. H. Arnaldo, and H. J. Radusch. 2012. Percolation behavior and mechanical properties of polycarbonate composites filled with carbon black/carbon nanotubes system. *Polimery* 57:204–211.
[13] Suin, S., N. K. Shrivastava, S. Maiti, and B. B. Khatua. 2013. Phosphonium modified organoclay as potential nanofiller for the development of exfoliated and optically transparent polycarbonate/clay nanocomposites: Preparation and characterization. *Eur. Polym. J.* 49:49–60.
[14] Jin, S. H., D. K. Choi, and D. S. Lee. 2008. Electrical and rheological properties of polycarbonate/multiwalled carbon nanotube nanocomposites. *Colloids Surf. A: Physicochem. Eng. Aspects* 313–314:242–245.
[15] Caponetti, E., L. Pedone, M. L. Saladino, D. C. Martino, and G. Nasillo. 2010. MCM-41-CdS nanocomposites materials. Preparation and characterization. *Microporous Mesoporous Mater.* 128:101–107.
[16] Saladino, M. L., E. Kraleva, S. Todorova, A. Spinella, G. Nasillo, and E. Caponetti. Synthesis and characterization of mesoporous Mn-MCM-41 materials. *J. Alloys Compd.* 509:8798–8803.
[17] Kurdakova, V., E. Quartarone, P. Mustarelli, A. Magistris, E. Caponetti, and M. L. Saladino. 2010. PBI-based composite membranes for polymer fuel cells. *J. Power Sources* 195:7765–7769.
[18] Araujo, S. A., A. S. Araujo, N. S. Fernandes, V. J. Fernandes Jr, and M. Ionashiro. 2010. Effect of the catalyst MCM-41 on the kinetics of the thermal decomposition of poly(ethylene terephthalate). *J. Therm. Anal. Calorim.* 99:465–469.
[19] Cerrada, M. L., E. Perez, J. P. Lourenco, J. M. Campos, and M. R. Ribeiro. 2009. Sustainable polyethylene/MCM-41 nanocomposites by in-situ polymerization. *Proceedings of the 12th International Conference on Mechanical and Technology of Composites Materials*, September 22–24, Varna, Bulgaria.
[20] Ver Meer, M. A., B. Narasimhan, B. H. Shanks, and S. K. Mallapragada. 2010. Effect of mesoporosity on thermal and mechanical properties of polystyrene/silica composites. *Appl. Mater. Interfaces* 2:41–47.
[21] Wang, N., Q. Fang, E. Chen, J. Zhang, and Y. Shao. 2009. Structure, crystallization behavior, and thermal stability of PP/MCM-41 nanocomposite. *Polym. Eng. Sci.* 49:2459–2466.
[22] Wang, N., Q. Fang, F. Zhang, E. Chen, and X. Zhang. 2011. Incorporation of nano-sized mesoporous MCM-41 materials used as fillers in natural rubber composite. *Mater. Sci. Eng. A* 528:3321–3325.
[23] Run, M. T., S. Z. Wu, D. Y. Zhang, and G. Wu. 2007. A polymer/mesoporous molecular sieve composite: Preparation structure and properties. *Mater. Chem. Phys.* 105:341–347.
[24] Lavall, R. L., S. Ferrari, C. Tomasi, M. Marzantowicz, E. Quartarone, M. Fagnoni, P. Mustarelli, and M. L. Saladino. 2012. MCM-41 silica effect on gel polymer electrolytes based on thermoplastic polyurethane. *Electrochim. Acta* 60:359–365.
[25] Mingtao, R., Z. Dayu, W. Sizhu, and W. Gang. 2007. Thermal decomposition of poly(ethylene terephthalate)/mesoporous molecular sieve composites. *Front. Chem. Eng. China* 1:50–54.
[26] Zhang, F. A., D. K. Lee, and T. J. Pinnavaia. 2009. PMMA-mesocellular foam silica nanocomposites prepared through batch emulsion polymerization and compression molding. *Polymer* 50:4768–4774.
[27] Zhang, F. A., D. K. Lee, and T. J. Pinnavaia. 2010. PMMA/mesoporous silica nanocomposites: Effect of framework stricture and pore size on thermomechanical properties. *Polym. Chem.* 1:107–113.

[28] Sibeko, M. A., M. L. Saladino, A. S. Luyt, and E. Caponetti. 2016. Morphology, mechanical and thermal properties of poly(methyl methacrylate) (PMMA) filled with mesoporous silica (MCM-41) prepared by melt compounding. *J. Mater. Sci.* 51:3957–3970.
[29] Imai, Y., A. Terahara, Y. Hakuta, K. Matsui, H. Hayashi, and N. Ueno. 2009. Transparent (bisphenol A carbonate)-based nanocomposites with high refractive index nanoparticles. *Eur. Polym. J.* 45:630–638.
[30] Gupta, M. C., and S. G. Viswanath. 1996. Role of metal oxide in the thermal degradation of bisphenol A polycarbonate. *J. Therm. Anal.* 46:1671–1679.
[31] Carrion, F. J., J. Sanes, and M. D. Bermudez. 2007. Influence of ZnO nanoparticles filler on the properties and wear resistance of polycarbonate. *Wear* 262:1504–1510.
[32] Motaung, T. E., M. L. Saladino, A. S. Luyt, and D. F. C. Martino. 2012. The effect of silica nanoparticles on the morphology, mechanical properties and thermal degradation kinetics of polycarbonate. *Compos. Sci. Technol.* 73:34–39.
[33] Wang, L., X. Han, J. Li, and D. Zheng. 2012. Preparation of modified mesoporous MCM-41 silica spheres and its application in pervaporation. *Powder Technol.* 231:63–69.
[34] Araujo, J. A., F. T. Cruz, I. H. Cruz, and D. Cardoso. 2013. Encapsulation of polmers in CTA-MCM-41 via microemulsion. *Microporous Mesoporous Mater.* 180:14–21.
[35] Michell, R. M., I. Blaszczyk-Lezak, C. Mijangos, and A. J. Müller. 2013. Confinement effects on polymer crystallization: From droplets to alumina nanopores. *Polymer* 54:4059–4077.
[36] Michell, R. M., I. Blaszczyk-Lezak, C. Mijangos, and A. J. Müller. 2014. Confined crystallization of polymers within anodic aluminum oxide templates. *J. Polym. Sci. B: Polym. Phys.* 52:1179–1194.
[37] Casas, M. T., R. M. Michell, I. Blaszczyk-Lezak, J. Puiggalí, C. Mijangos, A. T. Lorenzo, and A. J. Müller. 2015. Self-assembly of semicrystalline PE-*b*-PS diblock copolymers within AAO nanoporous templates. *Polymer* 70:282–289.
[38] Luyt, A. S., M. Messori, P. Fabbri, J. P. Mofokeng, R. Taurino, T. Zanasi, and F. Pilati. 2011. Polycarbonate reinforced with silica nanoparticles. *Polym. Bull.* 66:991–1004.
[39] Biswal, M., S. Mohanty, S. K. Nayak, and P. S. Kumar. 2013. Effect of functionalized nanosilica on the mechanical, dynamic-mechanical, and morphological performance of polycarbonate/nanosilica nanocomposites. *Polym. Eng. Sci.* 53:1287–1296.
[40] Menczel, J. D., and R. B. Prime. 2009. *Thermal Analysis of Polymers. Fundamentals and Applications.* New Jersey: Wiley. ISBN: 978-0-471-76917-0
[41] Climent, M. J., A. Corma, S. Iborra, M. C. Navarro, and J. Primo. 1996. Use of mesoporous MCM-41 aluminosilicates as catalysts in the production of fine chemicals: Preparation of dimethylacetals. *J. Catal.* 161:783–789.